J Therm Anal Calorim (2010) 99:829–834
DOI 10.1007/s10973-009-0479-4

Thermal study of some new quinolone ruthenium(III) complexes with potential cytostatic activity

Mihaela Badea · Rodica Olar · Dana Marinescu · Valentina Uivarosi · Teodor Octavian Nicolescu · Daniela Iacob

MEDICTA2009 Conference
© Akadémiai Kiadó, Budapest, Hungary 2009

Abstract A series of new complexes with mixed ligands of the type $RuL_m(DMSO)_nCl_3 \cdot xH_2O$ ((**1**) L: oxolinic acid (oxo), $m = 1$, $n = 0$, $x = 4$; (**2**) L: pipemidic acid (pip), $m = 2$, $n = 1$, $x = 2$; (**3**) L: enoxacin (enx), $m = 2$, $n = 1$, $x = 0$; (**4**) L: levofloxacin (levofx), $m = 2$, $n = 2$, $x = 8$; DMSO: dimethylsulfoxide) were synthesized and characterized by chemical analysis, IR and electronic data. Except oxolinic acid that behaves as bidentate, the other ligands (quinolone derivatives and DMSO) act as unidentate. Electronic spectra are in accordance with an octahedral stereochemistry. The thermal analysis (TG, DTA) in synthetic air flow elucidated the composition and also the number and nature of both water and DMSO molecules. The TG curves show 3–5 well-separated thermal steps. The first corresponds to the water and/or DMSO loss at lower temperatures followed either by quinolone thermal decomposition or pyrolisys at higher temperatures. The final product is ruthenium(IV) oxide.

Keywords DMSO · Quinolone · Ruthenium complex · Thermal behavior

M. Badea (✉) · R. Olar · D. Marinescu
Faculty of Chemistry, Department of Inorganic Chemistry, University of Bucharest, 90-92 Panduri Street, Sector 5, Bucharest 050663, Romania
e-mail: e_m_badea@yahoo.com

V. Uivarosi · T. O. Nicolescu · D. Iacob
Department of Inorganic Chemistry, Carol Davila University of Medicine and Pharmacy, 6 Traian Vuia Street, Bucharest, Romania

Introduction

The clinical use of platinum compounds was limited by the development of tumor resistance to the drugs [1–3] and by their side effects [4, 5]. These limitations caused further research to be oriented toward finding new, more active, less toxic, non-platinum anti-tumor agents based on other transition metals. Among of non-platinum compounds with anticancer properties, ruthenium complexes are very promising. Metal complexes of ruthenium(III) had shown ligand exchange kinetics similar to those of the platinum anti-tumor agents currently used in the clinic and exhibits a reduced toxicity [6]. Some study revealed that the presence in coordination sphere of easily exchangeable ligands allowed the interaction with DNA. For ruthenium complexes that behave as anti-tumor agents such kind of ligands are chloride ion, water, and DMSO [7–13]. The presence of solvent molecules (like water and DMSO) in the coordination sphere of ruthenium can be easily detected using the thermal analysis [14].

A series of quinolone metal complexes are already characterized [15–25] and in some cases their biological activity was investigated [26–28].

Based on these observations, new ruthenium(III) complexes with some quinolone anti-bacterials (oxolinic acid, pipemidic acid, enoxacin, and levofloxacin) have been synthesized and characterized by elemental analysis, spectral properties, and thermal analysis. The thermal analysis (TG and DTA) was performed in order to establish the thermal stability of these complexes during the pharmaceutical development studies. The thermal curves elucidated the composition and the number and nature of the solvent molecules also.

Experimental

Materials and methods

All chemicals were purchased from Sigma–Aldrich, reagent grade and were used without further purification.

The chemical analyses were performed on a Perkin Elmer PE 2400 analyzer (for C, H, N, and S) and an AAS Carl Zeiss Jena AAS1 spectrometer (for Ru).

IR spectra were recorded in KBr pellets with a FT-IR VERTEX 70 (Bruker) spectrometer in the range 400–4,000 cm^{-1}.

Electronic spectra by diffuse reflectance technique, with MgO as standard, were recorded in the range 300–1,500 nm, on a Jasco V 670 spectrophotometer.

The heating curves (TG and DTA) were recorded using a Labsys 1200 SETARAM instrument, with a sample mass of 6–15 mg over the temperature range of 20–900 °C, using a heating rate of 10 K/min. The measurements were carried out in synthetic air atmosphere (flow rate 16.66 cm^3/min) by using alumina crucibles.

Synthesis of the complexes and spectral data

A DMSO solution of ligand and $RuCl_3$ in a 2:1 molar ratio was heated under reflux for 6 h until the color turned into dark-brown. After cooling, a solution 2 M of NaCl has been added in order to obtain the solid product. The brown residue was filtered off and washed several times with distilled water and air dried.

*Complex Ru(oxo)Cl_3·4H_2O (**1**)*

Analysis, found: Ru, 18.35; C, 28.25; H, 3.71; N, 2.86%; calculated for $RuC_{13}H_{19}Cl_3NO_9$: Ru, 18.67; C, 28.83; H, 3.51; N, 2.58%; IR (KBr pellet), cm^{-1}: ν(OH), 3441s; $\nu(C{=}O)_c$, 1710s; $\nu(C{=}O)_p$, 1633s.

*Complex Ru(pip)$_2Cl_3$(DMSO)·2H_2O (**2**)*

Analysis, found: Ru, 10.35; C, 38.43; H, 8.31; N, 14.95; S, 3.73%; calculated for $RuC_{30}H_{44}Cl_3N_{10}O_9S$: Ru, 10.88; C, 38.8; H, 8.13; N, 15.08; S 3.44%; IR (KBr pellet), cm^{-1}: ν(OH), 3426s; $\nu(C{=}O)_c$, 1719s; $\nu(C{=}O)_p$, 1640s; ν(S=O), 1050m.

*Complex Ru(enx)$_2Cl_3$(DMSO) (**3**)*

Analysis, found: Ru, 10.48; C, 41.11; H, 4.62; N, 11.95; S, 3.68%; calculated for $RuC_{32}H_{40}Cl_3F_2N_8O_7S$: Ru, 10.91; C, 41.47; H, 4.32; N, 12.10; S 3.46%; IR (KBr pellet), cm^{-1}: $\nu(C{=}O)_c$, 1718m; $\nu(C{=}O)_p$, 1630s; ν(S=O), 1021m.

*Complex Ru(levofx)$_2Cl_3$(DMSO)$_2$·8H_2O (**4**)*

Analysis, found: Ru, 8.44; C, 39.84; H, 5.92; N, 6.43; S, 5.79%; calculated for $RuC_{40}H_{68}Cl_3F_2N_6O_{18}S_2$: Ru, 8.32; C, 39.54; H, 5.60; N, 6.92; S 5.27%; IR (KBr pellet), cm^{-1}: ν(OH), 3424s; $\nu(C{=}O)_c$, 1715m; $\nu(C{=}O)_p$, 1617s; ν(S=O), 1058m.

Results and discussion

Physico-chemical characterization of complexes

In this article, we report the preparation and physico-chemical characterization of some Ru(III) complexes with quinolone derivatives and DMSO (Fig. 1).

The major goal of this article was to characterize the spectral and thermal behavior of these complexes that

Fig. 1 The ligand formulas

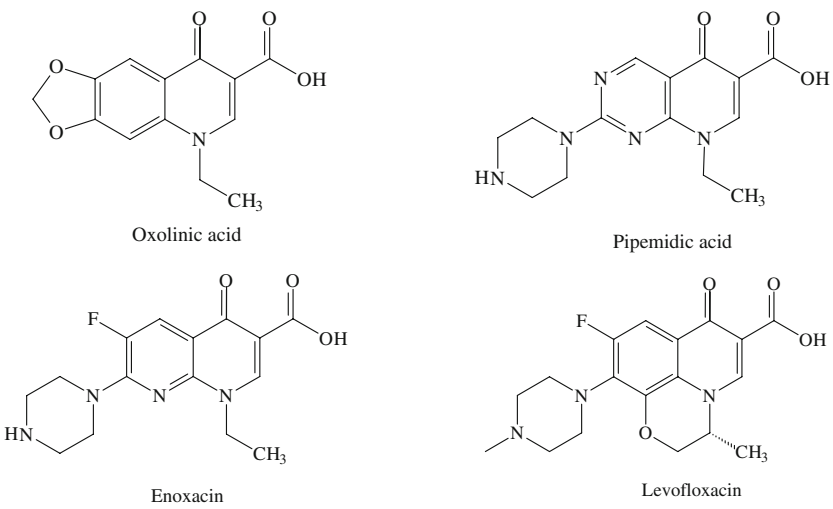

could behave as cytostatic agents. The complexes have been formulated on the basis of chemical analysis and IR spectra as it follows:

$[Ru(oxo)Cl_3(H_2O)](H_2O)_3$ (**1**)
$[Ru(pip)_2Cl_3(DMSO)](H_2O)_2$ (**2**)
$[Ru(enx)_2Cl_3(DMSO)]$ (**3**)
$[Ru(levofx)_2Cl_3(DMSO)]DMSO(H_2O)_8$ (**4**)

The compounds were obtained from the reaction of the $RuCl_3$ with quinolone derivatives in DMSO.

In the IR spectra of complexes the characteristic patterns of quinolone and DMSO are shown and indicate the unidentate coordination both for quinolone derivative and DMSO except for oxolinic acid that acts as bidentate. These common features are:

- The characteristic bands assigned to the both carboxylic and pyridonic carbonyl ($\nu(CO)_c$ and $\nu(CO)_p$), respectively, can be identified in all complexes spectra [29]. The position of these bands in complexes spectra indicate that the carbonyl and carboxyl groups are not involved in coordination;
- The bands which appear in 2,500–2,850 cm^{-1} range in ligands spectra can be assigned to $N^4_{(piperazyl)}$–H stretching vibrations. In the spectra of complexes these bands disappears probably due to the ligand coordination through the $N^4_{(piperazyl)}$ atom;
- The DMSO presence in complexes generates the appearance of a medium or strong band in 1,020–1,050 cm^{-1} range assigned to ν(S=O) stretching vibrations [30] characteristic to S-coordinated DMSO.

In the spectrum of complex (**1**) the bands assigned to $\nu(CO)_c$ and $\nu(CO)_p$ vibration modes are shifted to lower wavenumbers in comparison with oxolinic acid spectrum which is in accord with a chelate coordination via pyridonic and carboxylic oxygen atoms.

Electronic spectra of complexes display a large band with the absorption maxima in the range 400–530 nm and a shoulder in the range 550–700 nm that can be assigned to the spin allowed transition $^2T_2 \rightarrow {}^2A_2$, $^2T_1$ and spin forbidden one $^2T_2 \rightarrow {}^4T_1$ for Ru(III) with an octahedral stereochemistry [31].

On the basis of the above data the proposed coordination for the complexes is as it follows (Fig. 2):

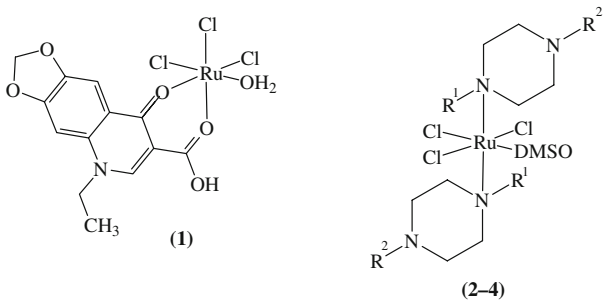

Fig. 2 The coordination sphere of complexes

Thermal behavior of complexes

The main objective of this article was to analyse the thermal behavior of the complexes having in view the composition confirmation and the solvent molecule role assessment.

The results concerning the thermal degradation of the new complexes are presented as it follows.

Thermal decomposition of $[Ru(oxo)Cl_3(H_2O)](H_2O)_3$

The TG and DTA curves corresponding to the complex (**1**) heated in the 20–900 °C temperature range indicate that decomposition follows four steps (Fig. 3).

The first step of compound transformation consists in an endothermic elimination of water (Table 1). The second step, exothermic, is not a single one being an overlapping of at least two processes as both TG and DTA curves indicate. This step corresponds to the partial oxolinic acid oxidative degradation consisting in 1,3-benzidioxole elimination (Fig. 4).

The resulted fragment 4-hydroxinicotinic acid remains coordinated through the both oxygen atoms from the carboxylic and carbonylic groups. The characteristic bands of the carboxylic and carbonylic groups at 1699 $\nu(CO)_c$ and 1635 cm^{-1} ($\nu(CO)_p$) appear shifted in the IR spectrum of this intermediate (Fig. 5b) in comparison with that of $Ru(oxo)Cl_3(H_2O)_4$ (Fig. 5a). Moreover the characteristic bands of the 1,3-benzidioxole disappear from this spectrum (1,224, ν(C–O–C); 939, ν(C–O) and 879 cm^{-1} γ(CH)).

Next step, exothermic also, corresponds to organic part loss in at least three processes according to TG curve. The resulted intermediate, $RuCl_3$, turns in RuO_2 in the last step,

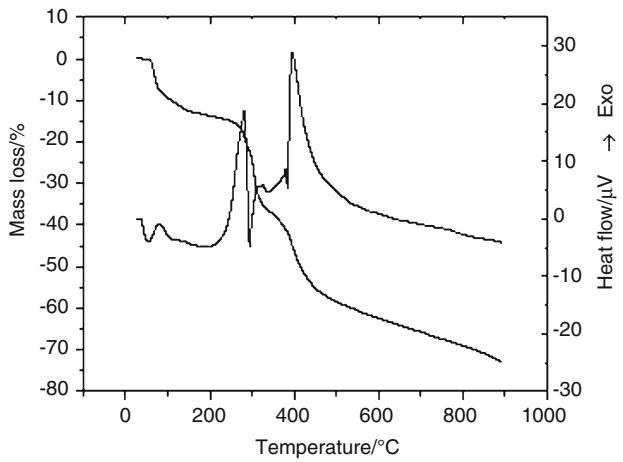

Fig. 3 TG and DTA curves of $[Ru(oxo)Cl_3(H_2O)](H_2O)_3$

Table 1 Thermal behavior data (in synthetic air atmosphere) for complexes

Complex	Step	Thermal effect	Temperature range/°C	Δm_{exp}/%	Δm_{calc}/%
$[Ru(oxo)Cl_3(H_2O)](H_2O)_3$ (**1**)	1.	Endothermic	51–136	13.4	13.3
	2.	Exothermic	205–350	22.5	22.6
	3.	Exothermic	350–515	25.8	25.7
	4.	Exothermic	515–900	13.7	13.8
$[Ru(pip)_2Cl_3(DMSO)](H_2O)_2$ (**2**)	1.	Endothermic	51–80	3.8	3.9
	2.	Endothermic	80–125	8.4	8.4
	3.	Exothermic	125–486	47.2	47.2
	4.	Exothermic	486–770	18.2	18.1
	5.	Exothermic	770–900	7.9	8.0
$[Ru(enx)_2Cl_3(DMSO)]$ (**3**)	1.	Endothermic	200–275	8.5	8.4
	2.	Exothermic	275–764	50.7	50.8
	3.	Exothermic	764–907	18.2	18.2
	4.	Exothermic	907–1000	8.1	8.0
$[Ru(levofx)_2Cl_3(DMSO)]DMSO(H_2O)_8$ (**4**)	1.	Endothermic	44–87	11.8	11.7
	2.	Endothermic	87–144	12.6	12.7
	3.	Exothermic	246–830	64.9	64.8

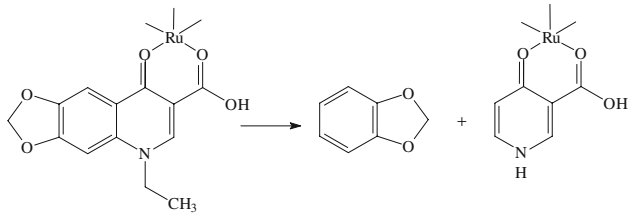

Fig. 4 The proposed second degradation step of complex (**1**)

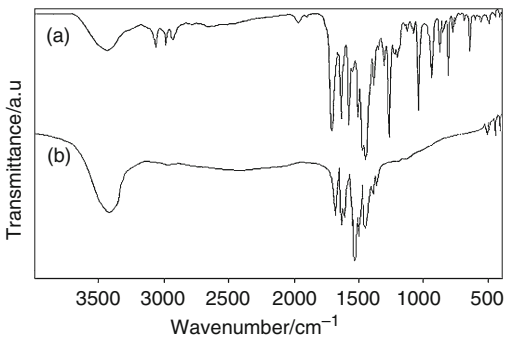

Fig. 5 IR spectra of $[Ru(oxo)Cl_3(H_2O)](H_2O)_3$ (*a*) and intermediate resulted at 350 °C (*b*)

process accompanied by an exothermic effect (found/calcd. overall mass loss: 75.4/75.4).

Thermal decomposition of $[Ru(pip)_2Cl_3(DMSO)](H_2O)_2$

Complex (**2**) decomposition occurs in five steps and begins with water elimination, process that proceeds at lower temperature (Table 1) [32–35]. The next step corresponds

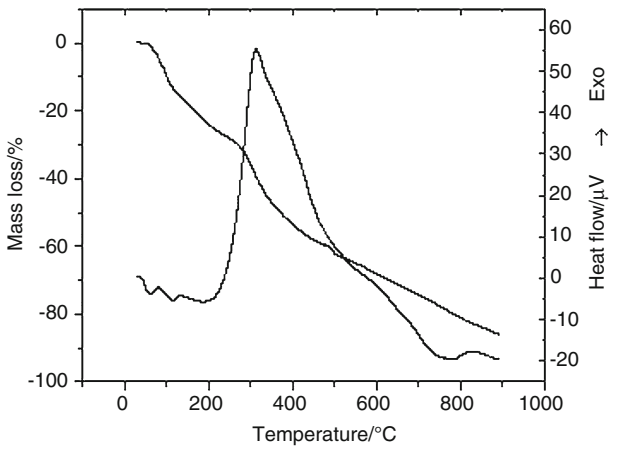

Fig. 6 TG and DTA curves of $[Ru(pip)_2Cl_3(DMSO)](H_2O)_2$

to the organic solvent (DMSO) loss (Fig. 6). The third step occurs with pipemidic acid degradation similar with that observed for other ruthenium(III) complexes with quinolone derivatives [14] (Fig. 7). The thermal degradation of pipemidic acid occurs in at least two successive processes as both TG and DTA indicate. In the fourth step the complex intermediate leads to $RuCl_3$ as a result of the tetrahydropyrazine oxidative degradation in at least two processes (according to both TG and DTA curves). The remaining $RuCl_3$ generates RuO_2 up to 900 °C (found/calcd. overall mass loss: 85.5/85.6).

Thermal decomposition of $[Ru(enx)_2Cl_3(DMSO)]$

The decomposition of complex (**3**) comprises also four steps and starts with DMSO elimination, process that

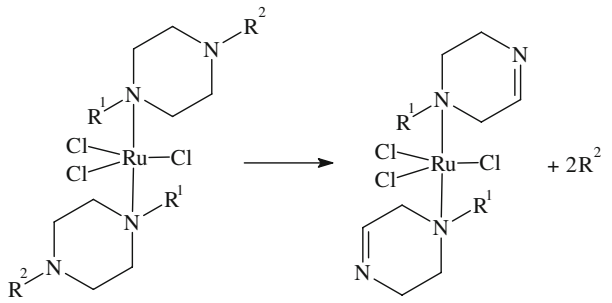

Fig. 7 The proposed second degradation step of complexes (**2**)–(**4**)

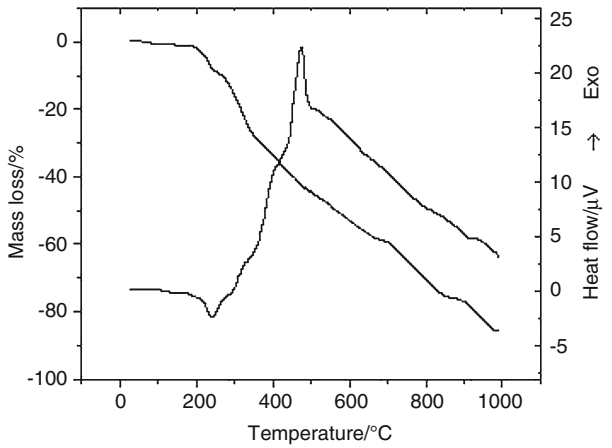

Fig. 8 TG and DTA curves of $[Ru(enx)_2Cl_3(DMSO)]$

occurs at high temperatures (Fig. 8). The second step exothermic is not a single one being formed by at least three processes, as indicate both TG and DTA curves. This step correspond to partial oxidative degradation of enoxacin, the fragment 1,4-diaza-1-cyclohexene remaining coordinated through N^4. The next steps are also complexes and consist in diamine elimination leading to $RuCl_3$ as intermediate. The final product is also RuO_2 (found/calcd. overall mass loss: 85.5/85.4).

Thermal decomposition of $[Ru(levofx)_2Cl_3(DMSO)]DMSO(H_2O)_8$

According to the TG profile (Fig. 9) the decomposition of $[Ru(levofx)_2Cl_3(DMSO)]DMSO(H_2O)_8$ (**4**) occurs in three, well-defined steps (found/calcd. overall mass loss: 89.3/89.2). After water loss in the 44–87 °C range, the DMSO elimination occurs in the second step. The resulted species is stable over a wide temperature range (144–246 °C). The final step, complex one, consists in at least two processes as both TG and DTA indicate, corresponding to levofloxacin stepwise oxidative degradation and chloride elimination. According to the mass variation the RuO_2 represents the final product of decomposition.

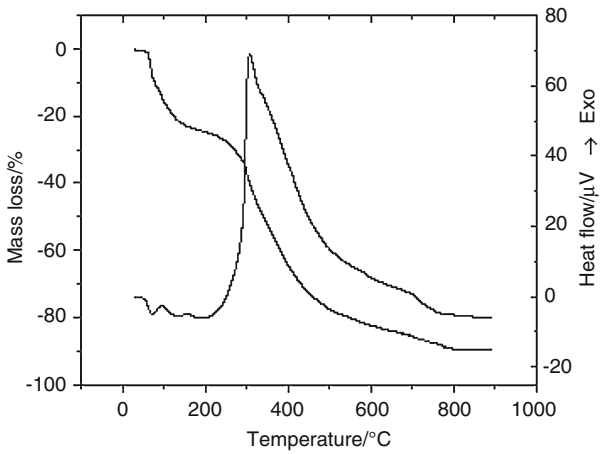

Fig. 9 TG and DTA curves of $[Ru(levofx)_2Cl_3(DMSO)]DMSO(H_2O)_8$

Conclusions

The new complexes of Ru(III) with quinolone as ligands belong to a class of coordination compounds of current interest having in view the cytostatic activity evidenced so far for similar species.

For all complexes quinolone derivative acts as unidentate except for oxolinic acid that is chelate coordinated according to IR data. The DMSO presence was evidenced for complexes (**2**)–(**4**).

Thermal analysis (TG, DTA) of these complexes elucidated the composition and also the number and nature of both water and DMSO molecules. The octahedral stereochemistry of complex $[Ru(oxo)Cl_3(H_2O)](H_2O)_3$ (**1**) can be completed by one coordinated water molecule. The higher temperature range (51–136 °C) corresponding to the water molecules loss sustains this supposition. For compounds (**2**) and (**4**) the water molecules are loss at lower temperatures (44–87 °C) indicating their crystallization role.

It was also evidenced the existence of an intermediate step corresponding to the thermal decomposition of quinolone derivatives. The nature of intermediates was evidenced by IR spectroscopy.

The final product is ruthenium (IV) oxide in all cases.

Acknowledgements This work was partially supported by the PNII grant nr. 61-048/2007 of the Romanian Ministry of Education and Research.

References

1. Kartalou M, Essigmann JM. Mechanisms of resistance to cisplatin. Mutat Res Fundam Mol Mech Mutag. 2001;478:23–43.
2. Wang D, Lippard SJ. Cellular processing of platinum anticancer drugs. Nat Rev Drug Discov. 2005;4:307–20.

3. Boulikas T, Vougiouka M. Cisplatin and platinum drugs at the molecular level. Oncol Rep. 2003;10:1663–82.
4. Rosenberg B. Noble metal complexes in cancer chemotherapy. Adv Exp Med Biol. 1977;91:129–50.
5. Hill JM, Speer RJ. Organo-platinum complexes as antitumor agents. Anticancer Res. 1982;2:173–86.
6. Brabec V, Novakova O. DNA binding mode of ruthenium complexes and relationship to tumor cell toxicity. Drug Resist Update. 2006;9:111–22.
7. Bergamo A, Gava B, Alessio E, Mestroni G, Serli B, Cocchietto M, et al. Ruthenium-based NAMI-A type complexes with in vivo selective metastasis reduction and in vitro invasion inhibition unrelated to cell cytotoxicity. Int J Oncol. 2002;21:1331–8.
8. Kostova I. Ruthenium complexes as anticancer agents. Curr Med Chem. 2006;13:1085–107.
9. Gallori E, Vettori C, Alessio E, González-Vílchez F, Vilaplana R, Orioli P, et al. DNA as a possible target for antitumor ruthenium(III) complexes: a spectroscopic and molecular biology study of the interactions of two representative antineoplastic ruthenium(III) complexes with DNA. Arch Biochem Biophys. 2000;376:156–62.
10. Messori L, Orioli P, Vullo D, Alessio E, Iengo E. A spectroscopic study of the reaction of NAMI, a novel ruthenium(III)anti-neoplastic complex, with bovine serum albumin. Eur J Biochem. 2000;267:1206–13.
11. Barca A, Pani B, Tamaro M, Russo E. Molecular interactions of ruthenium complexes in isolated mammalian nuclei and cytotoxicity on V79 cells in culture. Mutat Res Funda Mol Mech Mutag. 1999;423:171–81.
12. Sanna B, Debidda M, Pintus G, Tadolini B, Posadino AM, Bennardini F, et al. The anti-metastatic agent imidazolium *trans*-imidazoledimethylsulfoxide–tetrachlororuthenate induces endothelial cell apoptosis by inhibiting the mitogen-activated protein kinase/extracellular signal-regulated kinase signaling pathway. Arch Biochem Biophys. 2002;403:209–18.
13. Alessi E, Mestroni G, Bergamo A, Sava G. Ruthenium antimetastatic agents. Curr Top Med Chem. 2004;4:1525–35.
14. Badea M, Olar R, Marinescu D, Uivarosi V, Iacob D. Thermal decomposition of some biologically active complexes of ruthenium(III) with quinolone derivatives. J Therm Anal Calorim 2009. doi 10.1007/s10973-009-0343-6.
15. Zupančič M, Cerc Korošec R, Bukovec P. The thermal stability of ciprofloxacin complexes with magnesium(II), zinc(II) and cobalt(II). J Therm Anal Calorim. 2001;63:787–95.
16. Tarushi A, Psomas G, Raptopoulou CP, Kessissoglu DP. Zinc complexes of the antibacterial drug oxolinic acid: structure and DNA-binding properties. J Inorg Biochem. 2009;103:898–905.
17. Chen ZF, Xiong RG, Zuo J, Guo Z, You X, Fun HK, X-Ray crystal structures of Mg^{2+} and Ca^{2+} dimers of the antibacterial drug norfloxacin**.** Dalton Trans 2000:4013–5.
18. Chen ZF, Xiong RG, Zhang J, Chen XT, Xue ZL, You XZ. 2D molecular square grid with strong blue fluorescent emission: a complex of norfloxacin with zinc(II). Inorg Chem. 2001;40:4075–7.
19. Chen ZF, Li BQ, Xie YR, Xiong RG, You XZ, Feng XL. Synthesis, crystal structure, and characterization of mixed-ligand complex of copper(I) with drug of norfloxacin and triphenyl phosphine: $[Cu(PPh_3)_2(H\text{-}Norf)]ClO_4$. Inorg Chem Commun. 2001;4:346–9.
20. Wallis SC, Gahan LR, Charles BG, Hambley TW, Duckworth PA. Copper(II) complexes of the fluoroquinolone antimicrobial ciprofloxacin. Synthesis, X-ray structural characterization, and potentiometric study. J Inorg Biochem. 1996;62:1–16.
21. Gao F, Yang P, Xie J, Wang H. Synthesis, characterization and antibacterial activity of novel Fe(III), Co(II), and Zn(II) complexes with norfloxacin. J Inorg Biochem. 1995;60:61–7.
22. Mustafa J. Magnesium, calcium and barium perchlorate complexes of ciprofloxacin and norfloxacin. Acta Chim Slov. 2002;49:457–66.
23. Macias B, Villa M, Rubio I, Castineiras A, Borras J. Complexes of Ni(II) and Cu(II) with ofloxacin: Crystal structure of a new Cu(II) ofloxacin complex. J Inorg Biochem. 2001;84:163–70.
24. Choubey P, Singh P. Effect of chelation on antifungal activity of norfloxacin. Asian J Chem. 2002;14:1287–92.
25. Turel I, Globič A, Klavžar A, Pihlar B, Buglyo P, Tolis E, et al. Interactions of oxovanadium(IV) and the quinolone family member-ciprofloxacin. J Inorg Biochem. 2003;95:199–207.
26. Saha DK, Sandbhor U, Shirisha K, Padhye S, Deobagkar D, Anson CE, et al. A novel mixed-ligand antimycobacterial dimeric copper complex of ciprofloxacin and phenanthroline. Bioorg Med Chem Lett. 2004;14:3027–32.
27. Efthimiadou EK, Katsarou ME, Sanakis Y, Raptopoulou CP, Karaliota A, Katsaros N, et al. Neutral and cationic mononuclear copper(II) complexes with enrofloxacin: structure and biological activity. J Inorg Biochem. 2006;100:1378–88.
28. Efthimiadou EK, Thomadaki H, Sanakis Y, Raptopoulou CP, Katsaros N, Scorilas A, et al. Structure and biological properties of the copper(II) complex with the quinolone antibacterial drug *N*-propyl-norfloxacin and 2,2′-bipyridine. J Inorg Biochem. 2007;101:64–73.
29. Zupancic M, Turel I, Bukovec P, White AJP, Williams DJ. Synthesis and characterization of two novel zinc(II) complexes with ciprofloxacin. Crystal structure of $[C_{17}H_{19}N_3O_3F]_2{\cdot}[ZnCl_4]{\cdot}2H_2O$. Croat Chem Acta. 2001;74:61–74.
30. Nakamoto K. Infrared and raman spectra of inorganic and coordination compounds. New York: Wiley; 1986. p. 269.
31. Lever ABP. Inorganic electronic spectroscopy. Amsterdam, London, New York: Elsevier; 1986. p. 454.
32. Modi CK, Patel MN. Synthetic, spectroscopic and thermal aspects of some heterochelates. J Therm Anal Calorim. 2008;94:247–55.
33. Abou El-Enein SA. Polymeric and sandwich Schiff's bases complexes derived from 4,4′-methylenedianiline. Characterization and thermal investigation. J Therm Anal Calorim. 2008;91:929–36.
34. Gaber M, Rehab AF, Badr-Eldeen DF. Spectral and thermal studies of new Co(II) and Ni(II) hexaaza and octaaza macrocyclic complexes. J Therm Anal Calorim. 2008;91:957–62.
35. Vikram L, Sivasankar BN. Hydrazinium metal(II) and metal(III) ethylenediamine tetraacetate hydrates. Spectral, thermal and XRD studies. J Therm Anal Calorim. 2008;91:963–70.